Electron-Transfer Reactions of the Reductase Component of Soluble Methane Monooxygenase from *Methylococcus capsulatus* (Bath)†

Daniel A. Kopp, George T. Gassner, Jessica L. Blazyk, and Stephen J. Lippard*

Department of Chemistry, Massachusetts Institute of Technology, Cambridge, Massachusetts 02139

Received June 19, 2001; Revised Manuscript Received September 24, 2001

ABSTRACT: Soluble methane monooxygenase (sMMO) catalyzes the hydroxylation of methane by dioxygen to afford methanol and water, the first step of carbon assimilation in methanotrophic bacteria. This enzyme comprises three protein components: a hydroxylase (MMOH) that contains a dinuclear nonheme iron active site; a reductase (MMOR) that facilitates electron transfer from NADH to the diiron site of MMOH; and a coupling protein (MMOB). MMOR uses a noncovalently bound FAD cofactor and a [2Fe−2S] cluster to mediate electron transfer. The gene encoding MMOR was cloned from *Methylococcus capsulatus* (Bath) and expressed in *Escherichia coli* in high yield. Purified recombinant MMOR was indistinguishable from the native protein in all aspects examined, including activity, mass, cofactor content, and EPR spectrum of the [2Fe−2S] cluster. Redox potentials for the FAD and [2Fe−2S] cofactors, determined by reductive titrations in the presence of indicator dyes, are $FAD_{ox/sq}$, -176 ± 7 mV; $FAD_{sq/hq}$, -266 ± 15 mV; and $[2Fe-2S]_{ox/red}$, -209 ± 14 mV. The midpoint potentials of MMOR are not altered by the addition of MMOH, MMOB, or both MMOH and MMOB. The reaction of MMOR with NADH was investigated by stopped-flow UV−visible spectroscopy, and the kinetic and spectral properties of intermediates are described. The effects of pH on the redox properties of MMOR are described and exploited in pH jump kinetic studies to measure the rate constant of 130 ± 17 s^{-1} for electron transfer between the FAD and [2Fe−2S] cofactors in two-electron-reduced MMOR. The thermodynamic and kinetic parameters determined significantly extend our understanding of the sMMO system.

Methanotrophic bacteria use methane as their sole source of carbon and energy. These organisms are of interest for their role in regulating atmospheric concentrations of methane, a potent greenhouse gas (*1*), and for environmental bioremediation applications (*2*, *3*). Chemists are intrigued by the ability of methanotrophs to oxidize methane selectively to methanol in buffered aqueous solution, using dioxygen as the oxidant at ambient pressure and temperature. Methane monooxygenase, the enzyme system that catalyzes this remarkable transformation, has been scrutinized for over two decades (*4*−*8*).

Two classes of MMO have been identified, a copper-containing, membrane-bound (particulate) form referred to as pMMO (*9*) and a soluble form, sMMO, that contains nonheme iron. The sMMO from *Methylococcus capsulatus* (Bath) uses three proteins to carry out the reaction in eq 1. MMOH is a 251 kDa multimeric hydroxylase that houses a carboxylate-bridged diiron active site in each of its two α subunits. Reducing equivalents are delivered to the active sites of MMOH by MMOR, a 38.5 kDa protein with FAD and [2Fe−2S] cofactors. A 15.9 kDa coupling protein termed MMOB serves to couple oxidation of NADH to methane hydroxylation (*7*, *8*, *10*).

$$CH_4 + O_2 + NADH + H^+ \rightarrow CH_3OH + NAD^+ + H_2O \quad (1)$$

The catalytic cycle of sMMO is illustrated in Scheme 1. A complex of the reduced, diiron(II) MMOH and MMOB reacts with dioxygen, proceeding through a series of spectroscopically characterized, transient intermediates (*11*, *12*). A diiron(IV) species is believed to be responsible for the hydroxylation of methane (*11*, *13*). In the final stages of the reaction cycle, the diiron(III) centers of MMOH are reduced by intermolecular electron transfer from MMOR, and methanol is discharged from the active site. The methane and dioxygen activation steps of the sMMO reaction have

† This work was supported by National Institutes of Health Research Grant GM32134 (S.J.L.). D.A.K. is a National Institutes of Health biotechnology predoctoral trainee, G.T.G. was supported by an NIH postdoctoral fellowship, and J.L.B. is a Howard Hughes Medical Institute predoctoral fellow.

* To whom correspondence should be addressed. E-mail: lippard@lippard.mit.edu. Telephone: (617) 253-1892. Fax: (617) 258-8150.

[1] Abbreviations: MMO, methane monooxygenase; pMMO, particulate MMO; sMMO, soluble MMO; MMOH, hydroxylase component of sMMO; MMOR, reductase component of sMMO; MMOB, coupling protein of sMMO; FAD_{ox}, FAD_{sq}, and FAD_{hq}, flavin adenine dinucleotide in its oxidized, semiquinone, and hydroquinone oxidation states, respectively; $MMOR_{2e-}$, MMOR reduced by two electrons; NAD^+ and NADH, oxidized and reduced forms of nicotinamide adenine dinucleotide; Fd, ferredoxin; FNR, ferredoxin:$NADP^+$ reductase; PDR, phthalate dioxygenase reductase; E_3, CDP-6-deoxy-L-*threo*-D-*glycero*-4-hexulose-3-dehydrase reductase; MES, 2-(*N*-morpholino)ethanesulfonic acid; MOPS, 3-(*N*-morpholino)propanesulfonic acid; TAPS, *N*-(tris(hydroxymethyl)methyl)-3-aminopropanesulfonic acid; E_{FeS}, midpoint potential of the MMOR $[2Fe-2S]_{ox}/[2Fe-2S]_{red}$ redox couple; E_{FAD1}, midpoint potential of the MMOR FAD_{ox}/FAD_{sq} redox couple; E_{FAD2}, midpoint potential of the MMOR FAD_{sq}/FAD_{hq} redox couple.

10.1021/bi015556t CCC: $20.00
Published on Web 11/10/2001

Scheme 1

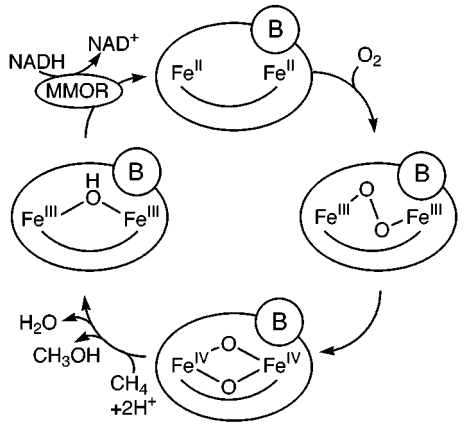

been extensively studied, but until now the electron-transfer reactions required for catalysis have received little attention.

MMOR has been grouped with other electron-transfer proteins, including Fd and FNR, PDR, E_3, nitrate reductase, cytochrome b_5 reductase, and cytochrome P450 reductase, on the basis of function and sequence homology (*14*, *15*). Other bacterial mono- and dioxygenases have related systems, including alkene monooxygenase and phenol hydroxylase (*16*−*19*). These proteins all use a flavin to convert reducing equivalents between the two-electron currency of NAD(P)H and the single-electron units required by metal centers.

In this article we report a high-yield recombinant expression system for MMOR, which was instrumental for investigating its electron-transfer reactions. The yields of MMOR purified from *M. capsulatus* (Bath) are insufficient to carry out extensive studies of this kind. With a means to obtain large quantities of highly purified MMOR at our disposal, we investigated thermodynamic and kinetic properties of its interactions with NADH. The distribution of electrons between FAD and [2Fe−2S] cofactors in $MMOR_{2e-}$ was also examined, as was the effect of pH on this distribution. The redox potentials of the MMOR cofactors were determined relative to one another as a function of pH. By pH jump methodology, we measured the rate constant for electron transfer between the FAD and [2Fe−2S] cofactors, providing the first direct determination of an isolated electron-transfer step in the sMMO reaction cycle. The results of these studies are described herein.

MATERIALS AND METHODS

Materials and General Methods. Taq DNA polymerase was obtained from Gibco BRL (Gaithersburg, MD), restriction enzymes *Eco*RI and *Hin*dIII were from New England Biolabs (Beverly, MA), plasmid pKK223-3 was from Amersham Pharmacia Biotech (Piscataway, NJ), and alkaline phosphatase was from Boehringer Mannheim (Indianapolis, IN).

The FAD content of MMOR was determined by boiling a sample of the protein for 3 min, centrifuging for 5 min at 10 000*g* to pellet the denatured protein, and measuring the optical spectrum of the supernatant using $\epsilon_{450}^{FAD} = 11\,300$ M^{-1} cm^{-1}. Iron determinations were made by the ferrozine method (*20*, *21*). EPR spectra were recorded with a Bruker EMX spectrometer fitted with an Oxford ESR 900 liquid-helium cryostat. UV−visible spectra were obtained with an HP 8453 diode array spectrophotometer.

Cloning of MMOR. The *mmoC* gene, which codes for MMOR, was amplified with *Taq* DNA polymerase from the pCH4 plasmid, obtained from J. C. Murrell (*22*), by using the following primers: 5′-CG*GAATTC*AACATTAAGGAG-GTAAATTTATGCAGCGAG-3′ and 5′-TCACAGTACT-T*AAGCTT*TTCAGGCCGCCCCGGAC-3′, which introduced *Eco*RI and *Hin*dIII sites, respectively, at the ends of the 1093-bp amplified gene. The resulting PCR product was digested with *Eco*RI and *Hin*dIII, as was the expression plasmid pKK223-3. The plasmid digest was treated with alkaline phosphatase, extracted with phenol−chloroform, and precipitated with ethanol prior to ligation. Ligation products were transformed into *E. coli* XL1-Blue cells, and transformants were selected on LB-ampicillin (Ap, 100 μg/mL) plates. Five positive clones were identified, each containing a correctly sized insert as judged by restriction digest analysis.

Sequencing of one positive clone, pRED(AP14), revealed a point mutation in the *mmoC* coding region of this plasmid that would give rise to a T123I change in the protein sequence. Site-directed mutagenesis using the QuikChange protocol (Stratagene, La Jolla, CA) was performed on pRED-(AP14) with the primers 5′-GCAGCGAGTTCAC*A*CTAT-CACGGCGGTG-3′ and 5′-CACCGCCGTGATAG*T*GT-GAACTCGCTGC-3′. Isolation and sequencing of the resulting plasmid, pRED-K2, revealed that it contained the native *mmoC* sequence (*22*, *23*).

Expression and Purification of Recombinant MMOR. The expression plasmid pRED-K2 was transformed into *E. coli* JM105 cells. Cells were grown to saturation at 37 °C and with 200 rpm shaking in 100 mL of LB-Ap (100 μg/mL) medium. The saturated culture was diluted 100-fold into six 1 L quantities of LB-Ap (100 μg/mL). When the culture reached an OD_{600} of 0.4, 1.0 mL of a freshly prepared and filter-sterilized 100 mM solution of $Fe(NH_4)_2(SO_4)_2 \cdot 6H_2O$ was added to each 1 L of medium. MMOR expression was induced at OD_{600} of 0.6 by adding IPTG to a final concentration of 1 mM. Expression was continued for an additional 3.5 h before the cells were harvested. The cells were disrupted by sonication, and insoluble debris was removed by centrifugation at 100 000*g* for 35 min. After passage through 0.2 μm membranes, the soluble fraction was applied to a DEAE-Sepharose CL6B (Amersham Pharmacia) column (2.6 × 15 cm) equilibrated in buffer A (20 mM Tris, pH 7.0, 8 mM sodium thioglycolate, and 50 mM NaCl). Proteins were eluted with an 800 mL gradient of buffer A to buffer B (20 mM Tris, pH 7.0, 8 mM sodium thioglycolate, and 500 mM NaCl). MMOR eluted at approximately 380 mM NaCl. Fractions containing MMOR, as determined by their optical spectra and SDS−PAGE analysis, were pooled and concentrated by ultrafiltration. Further purification was carried out by affinity chromatography on a 5′-AMP Sepharose (Sigma) column (2.6 × 11 cm). After application of MMOR to this column, contaminating proteins were washed off with 100 mL of buffer A. Most of this fraction (∼80−90%) consisted of MMOR lacking FAD but containing an intact [2Fe−2S] cluster. Elution with buffer B containing 1 mM NADH afforded >95% pure MMOR, as judged by SDS−PAGE, containing both FAD and [2Fe−2S] cofactors. Pure protein was exchanged into 25 mM

MOPS, pH 7.0, 1 mM DTT buffer with a Biogel P6 desalting column. A typical preparation yielded 15 mg of pure MMOR/L of starting *E. coli* culture. Samples for mass spectrometry were prepared as in ref *23*.

Redox Potential Determination. The midpoint potentials of the $FAD_{ox/sq}$, $FAD_{sq/hq}$, and $[2Fe-2S]_{ox/red}$ couples of MMOR were determined with a series of reductive titration experiments in the presence of redox indicator dyes. Each titration included approximately 30 μM MMOR and dye in 1 mL of 50 mM potassium phosphate buffer, pH 7.0, at 25 °C. The indicators were phenosafranine ($E^{\circ\prime} = -252$ mV), anthraquinone-2-sulfonate ($E^{\circ\prime} = -226$ mV), anthraquinone-2,6-disulfonate ($E^{\circ\prime} = -184$ mV), and anthraquinone-1,5-disulfonate ($E^{\circ\prime} = -174$ mV). Titrations with the high potential anthraquinone disulfonate dyes were very slow to reach equilibrium. To circumvent this problem, titrations with high potential dyes were performed with a small concentration (~10% relative to the anthraquinone dye) of phenosafranine.

Aliquots of 1−2 mM sodium dithionite were added by means of a gastight Hamilton syringe equipped with a repeating dispenser. Titrations were carried out in a sealed quartz cuvette under an anaerobic nitrogen atmosphere. UV−visible spectra were recorded after each addition, allowing 3−10 min for equilibration.

Data were processed by first correcting the spectra for dilution and then subtracting the starting (oxidized) spectrum from each spectrum of the titration. Each difference spectrum was then fit as a linear combination of component spectra (KaleidaGraph 3.0, Synergy Software, Reading, PA), as shown in eq 2. The component spectra, represented by $\Delta\epsilon_i(\lambda)$ in eq 2, correspond to the absorption spectral differences for the reduced minus the oxidized states of each chromophore for $380 < \lambda < 800$ nm.

$$\Delta A(\lambda) = \Sigma \Delta\epsilon_i(\lambda)(\Delta c_i) \tag{2}$$

Initial protein and dye concentrations were determined by fitting the starting spectrum to a linear combination of oxidized protein and dye spectra to make the analysis internally consistent and eliminate any errors due to inaccurate extinction coefficients. The chromophores considered were FAD_{ox}, FAD_{sq}, FAD_{hq}, $[2Fe-2S]_{ox}$, $[2Fe-2S]_{red}$, dye_{ox}, and dye_{red}. The dye and [2Fe−2S] spectra were determined experimentally by titrating the dyes or the MMOR−Fd domain with dithionite; component spectra of the MMOR−FAD domain were determined by evolving factor analysis (Specfit, Spectrum Software Associates, Marlborough, MA) of a reductive titration (*24*).

Concentration differences were converted to ratios of reduced/oxidized chromophores according to eq 3. The solution potential was calculated from the ratio of reduced to oxidized dye and related to the midpoint potential of one of the MMOR cofactors by the Nernst relationship, eq 4. In principle, each spectrum of a titration provides a measurement of the midpoint potential for each redox couple of MMOR. In practice, only those spectra for which the solution potential, dye midpoint potential, and estimated MMOR potential fell within 40 mV of one another were used in calculating the midpoint potentials of the cofactors.

$$\frac{c_{i,\mathrm{red}}}{c_{i,\mathrm{ox}}} = \frac{\Delta c_i}{c_{i,\mathrm{total}} - \Delta c_i} \tag{3}$$

$$E = E^{\circ\prime}{}_{\mathrm{dye}} - \frac{RT}{n_{\mathrm{dye}}F}\ln\left(\frac{[\mathrm{dye}_{\mathrm{red}}]}{[\mathrm{dye}_{\mathrm{ox}}]}\right) = E^{\circ\prime}{}_{i} - \frac{RT}{n_i F}\ln\left(\frac{[i_{\mathrm{red}}]}{[i_{\mathrm{ox}}]}\right) \tag{4}$$

Relative redox potentials at various pH values were determined as above, except that no indicator dyes were included. The difference spectra were fit with component spectra that had been determined at the relevant pH (*24*). Without indicator dye, the solution potential is unknown; thus, the redox potential of each couple was determined relative to the other redox couples of MMOR. The pK_a values determined from these data were obtained by fitting to equations following the form of eq 6 (see below).

Stopped-Flow Experiments. A Hi-Tech model SF-61 DX2 was used for all experiments, equipped with either a photomultiplier and a tungsten lamp for single-wavelength mode or a diode array detector using a 75 W xenon arc lamp for multiwavelength illumination. The flow system was first made anaerobic by flushing with a solution of sodium dithionite; alternatively, glucose oxidase, catalase, and 1 mM glucose were employed. Anaerobic buffer was then used to rinse the flow system. MMOR was made anaerobic by 8−10 cycles of vacuum gas exchange with O_2-free N_2. NADH solutions were made anaerobic by purging with N_2 for at least 20 min. Experiments were thermostated at 4 °C. Concentrations of MMOR were in the 10−25 μM range and NADH concentrations were ~10 times that of MMOR, except when otherwise specified. Where MMOB was included, it was loaded in the syringe with NADH. Data were fit (eq 5) to a sum of three or four exponential decays, as appropriate.

$$\mathrm{abs}_\lambda(t) = \Sigma A_i \exp(-k_i t) + C \tag{5}$$

Analysis of Diode Array Spectra. Diode array spectra of $MMOR_{2e-}$, recorded between 1 and 2 s after mixing MMOR and NADH as described above, were fit as a sum of component spectra, with the following additional constraints. The concentration of FAD_{sq} was equal to the concentration of $[2Fe-2S]_{red}$, and the total concentration of [2Fe−2S] was equal to the total concentration of FAD. In $MMOR_{2e-}$, the two electrons can reside either both on FAD (FAD_{hq}) or one on FAD and one on the [2Fe−2S] cluster; for this reason, the concentrations of FAD_{sq} and $[2Fe-2S]_{red}$ must in principle always be equal in $MMOR_{2e-}$.

Procedures for Variable-pH Experiments. For experiments in which the pH was varied, MMOR was prepared in 1 mM MOPS, pH 7.0, and mixed with strongly buffered solutions at the desired pH. Buffers used were 50 mM MES for $5.27 \leq \mathrm{pH} \leq 6.30$, 50 mM MOPS for $6.31 \leq \mathrm{pH} \leq 7.50$, and 50 mM TAPS for $7.51 \leq \mathrm{pH} \leq 8.50$. Constant ionic strength of 100 mM was maintained in all solutions by addition of NaCl.

To determine the pK_a associated with pH-dependent effects on the reaction of MMOR with NADH, the change in absorbance at 625 nm over 1 s was recorded with the stopped-flow instrument. The data were fit to a sum of three exponentials, and the fit parameters were used to calculate A_{625} at $t = 0$ s and $t = 1$ s. The difference between these

Table 1: Properties of Native and Recombinant MMOR

	native MMOR	recombinant MMOR
MW measd[a] (Da)	38 545.6[b] ± 3.9	38 546.9 ± 3.9
Fe content (mol/mol of protein)	1.92[c]	2.06 ± 0.05
FAD content (mol/mol of protein)	1.00[c]	1.1 ± 0.1
λ_{max} (nm), pH 7.0, 25 °C	334, 394, 458	334, 394, 458
g values (fully reduced)	2.047, 1.960, 1.864[c]	2.047, 1.958, 1.871[d]

[a] Expected 38 542.6 Da for apoprotein with N-terminal methionine intact. [b] As reported in ref *23*. [c] As reported in ref *25*. [d] EPR recorded at 10 K, 50 μW, and 25.7 G modulation amplitude.

two values was computed and plotted as a function of pH. The relationship defined in eq 6 was used to fit these data and determine the pK_a, where ΔA_{max} and ΔA_{min} are the maximum and minimum values of ΔA_{625}, respectively.

$$A = \Delta A_{max} - \frac{\Delta A_{max} - \Delta A_{min}}{1 + 10^{(pH - pKa)}} \quad (6)$$

A double-mixing pH jump experiment was carried out by first mixing 160 mM MMOR with 160 mM NADH to generate $MMOR_{2e-}$, followed by mixing with a buffer of different pH after a 1 s delay. To jump to a higher pH value, MMOR and NADH were prepared in 50 mM MES (pH 5.79) and mixed with 50 mM TAPS (pH 9.68). The final pH of the mixture was 8.10. To jump to a lower pH, MMOR and NADH were prepared in 50 mM TAPS (pH 8.02) and mixed with 50 mM MES (pH 4.82). The final mixture had a pH of 5.78.

RESULTS

Characterization of Recombinant MMOR. Several experimental results establish the identity of recombinant MMOR with that isolated from the native *M. capsulatus* (Bath) bacteria. Table 1 compares important parameters for native and recombinant MMOR. The cofactor content of recombinant MMOR was determined to be 1.1 ± 0.1 FAD- and 2.06 ± 0.05 Fe/mol of protein, respectively, in agreement with literature values (*25*). The UV−visible spectrum was the same as that of native MMOR. Substituting recombinant MMOR for native MMOR in sMMO activity assays afforded identical results. Mass spectrometric analysis gave a molecular weight within experimental error of the computed value for the apoprotein with the N-terminal methionine intact (see also ref *23*). In addition, the EPR spectrum of fully reduced recombinant MMOR shows a rhombic signal characteristic of a mixed valence $[2Fe-2S]^+$ cluster with *g* values very close to those observed for native MMOR (*26*).

Redox Potentials of MMOR. Selected difference spectra obtained from a reductive titration of MMOR in the presence of the indicators phenosafranine and anthraquinone-2,6-disulfonate are shown in Figure 1. For a titration with a single dye, fitting to the difference spectra required fewer independent variables (four) than for fits to the raw spectra (seven). The calculated midpoint potentials for the three redox couples are displayed in Table 2.

Redox potentials of MMOR were also measured in the presence of the other two sMMO components (Table 2). Complexes of the type MMOH/2MMOR and MMOH/2MMOR/2MMOB were examined, as was an equimolar mixture of MMOR and MMOB. The potentials of MMOR in the complexes do not change from those of free MMOR, within the error of the measurements. Although MMOH forms complexes with MMOR and MMOB, the latter two do not interact with one another (*10*, *27*).

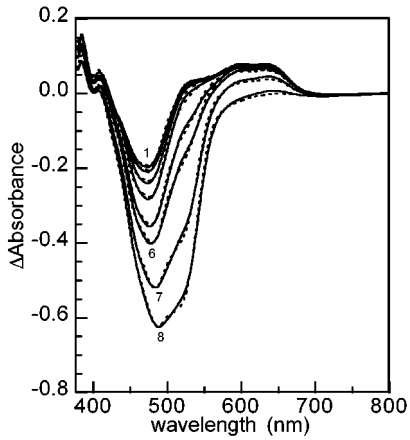

FIGURE 1: Difference spectra for the reductive titration of a 1 mL mixture of 29 μM MMOR, 3.8 μM phenosafranine, and 39 μM anthraquinone-2,6-disulfonate by dithionite. Spectra 1−8 correspond to the addition of 110, 130, 150, 170, 190, 210, 220, and 240 μL, respectively, of a solution of ~1 mM sodium dithionite. Fits (dashed lines) are superimposed on the data over the wavelength range 380−800 nm.

Kinetic Behavior of MMOR Reduction by NADH. The reaction of oxidized MMOR with NADH was investigated by stopped-flow optical spectroscopy. Preliminary studies of this reaction were reported previously (*10*, *28*, *29*), and spectra of intermediates in the reaction were derived from fits to the diode array kinetic traces (*10*). Figure 2A shows the time-dependent changes in absorbance at three wavelengths, 458, 625, and 740 nm. Fits to these changes are superimposed on the data, reflecting the steps outlined in Scheme 2. The reduction chemistry begins with NADH binding to MMOR to produce a species with a charge-transfer interaction between the nicotinamide ring of NADH and the flavin isoalloxazine. The charge-transfer intermediate, termed CT1, has a visible band centered at about 575 nm (Figure 2B). Transfer of hydride produces NAD^+ and the reduced flavin (FAD_{hq}). The resulting species, CT2, has a more intense charge-transfer band that is red-shifted (λ_{max} ~ 740 nm) relative to that of CT1 (Figure 2B). Formation of CT2 is apparent in Figure 2A as an increase in A_{740} at t < 8 ms. Release of NAD^+ is observed by the disappearance of the CT2 band, which occurs simultaneously with electron transfer from FAD_{hq} to $[2Fe-2S]_{ox}$. The NAD^+ release phase appears in Figure 2A as a decrease in A_{740} for t > 10 ms, due to loss of the charge-transfer interaction between NAD^+ and FAD_{hq} and the continuing increase in A_{625} arising from the increasing concentration of FAD_{sq}. The final species, SQ, has a spectrum characteristic of FAD_{sq} and $[2Fe-2S]_{red}$ (Figure 2B).

Table 2: Midpoint Potentials at 25 °C and pH 7.0 of MMOR Alone and in Complexes with Other sMMO Proteins

	$FAD_{ox/sq}$ (mV)	$[2Fe-2S]_{ox/red}$ (mV)	$FAD_{sq/hq}$ (mV)
MMOR native[a]	-150 ± 20	-220 ± 20	-260 ± 5
MMOR recombinant	-176 ± 7	-209 ± 14	-266 ± 15
MMOR + MMOB	-178 ± 1	-200 ± 6	-255 ± 4
MMOH/2MMOR	-167 ± 14	-207 ± 5	-260 ± 9
MMOH/2MMOB/2MMOR	-160 ± 2	-208 ± 6	-258 ± 8

[a] As reported in ref *26*.

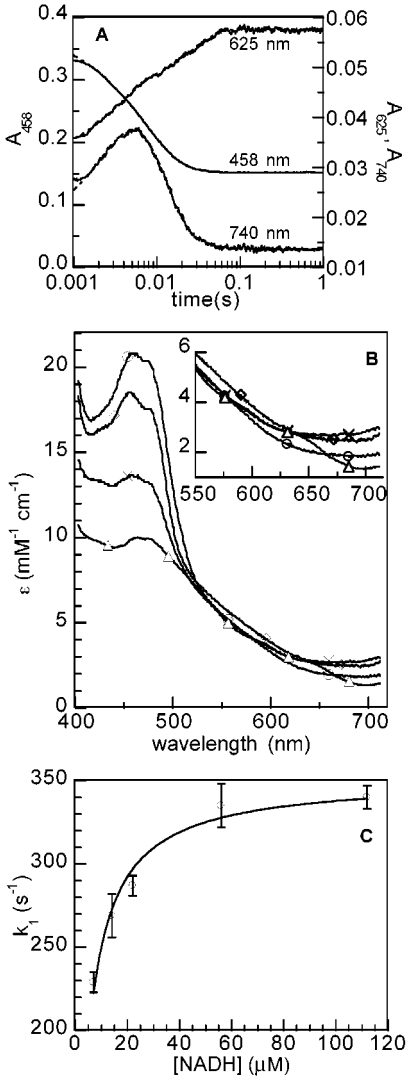

FIGURE 2: Reaction of $MMOR_{ox}$ with NADH studied by stopped-flow UV−visible spectroscopy. (A) Time-dependent absorbance changes at 458, 625, and 725 nm during the reaction of 20 μM $MMOR_{ox}$ with 200 μM NADH at 4 °C. Dashed lines are fits to eq 5. (B) Derived spectra of species (circles, $MMOR_{ox}$; diamonds, CT1; crosses, CT2; triangles, SQ) observed in the reaction. Species $MMOR_{ox}$, CT1, CT2, and SQ are defined in Scheme 2. (C) Dependence of k_1 (Scheme 2) on the concentration of NADH.

The reduction kinetics of MMOR were also measured in the presence of MMOB. Addition of 1−5 equiv of MMOB to the reaction of MMOR with NADH had no effect on the reaction rates or spectra of the intermediates.

Complexes of MMOR with NAD(H). The binding that was observed upon mixing MMOR with NADH was originally modeled as a single step with an observed rate constant (*10*). Investigation of the NADH concentration dependence of this reaction, however, reveals that binding occurs in more than one step. Specifically, the rate constant for the formation of the first observed intermediate, CT1, can be saturated (Figure 2C). This result implies the existence of a spectroscopically silent species that forms prior to CT1. This species is termed MC1 for Michaelis complex 1 (Scheme 2). A fit to the data reveals a K_d value of 3.8 μM for NADH binding to oxidized MMOR.

Scheme 2

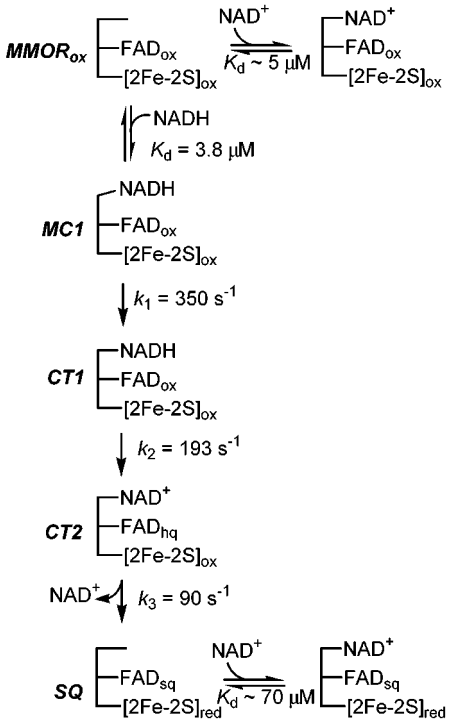

To investigate the binding of NAD^+ to oxidized MMOR, the kinetics of the reaction of MMOR with NADH were studied in the presence of varying concentrations of NAD^+ and at three different wavelengths (Figure 3). As expected, the reaction is inhibited by NAD^+. The data were modeled according to Scheme 2 with HopKINSIM (*30*, *31*). The K_d value for NAD^+ binding to $MMOR_{ox}$ was estimated to be ~5 μM. In addition, the K_d value for NAD^+ binding to two-electron-reduced MMOR was estimated from the absorbance changes at 725 nm at 1 s after mixing (Figure 3C) to be 70 ± 24 μM. Increased absorbance at 725 nm at 1 s is due to the formation of a CT2-type charge-transfer complex between $MMOR_{2e-}$ and excess NAD^+.

Effect of pH on the Reaction of MMOR and NADH. This reaction was also examined in buffers at 12 different pH values in the range 5.3−8.3. Below pH 5.0, MMOR precipitates from solution; thus, the pH was kept above this value to ensure that no protein precipitated in the stopped-flow spectrometer. Figure 4A shows that, at high pH, the final value of A_{625} is significantly larger than at low pH. It

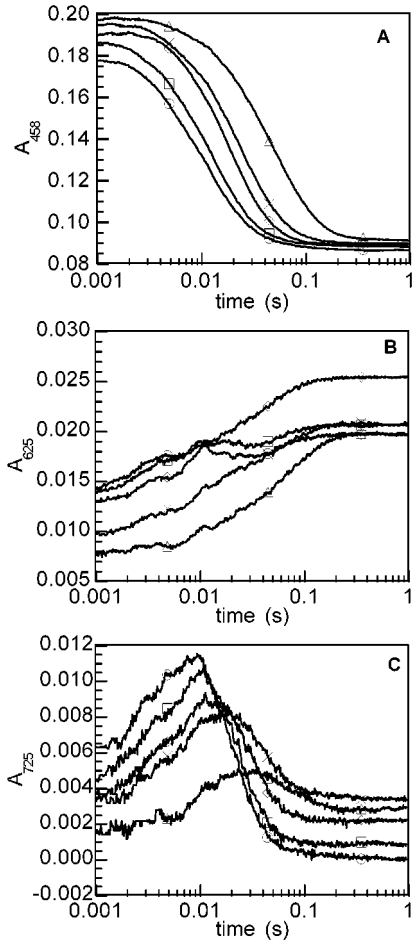

FIGURE 3: Product inhibition of reaction of $MMOR_{ox}$ and NADH. Time-dependent absorbance changes were recorded at 458 nm (A), 625 nm (B), and 725 nm (C) by allowing a 22.4 μM $MMOR_{ox}$ solution to react with 224 μM NADH in the presence of varying concentrations (circles, 0 μM; squares, 62.5 μM; diamonds, 250 μM; crosses, 500 μM; triangles 1.5 mM) of NAD^+.

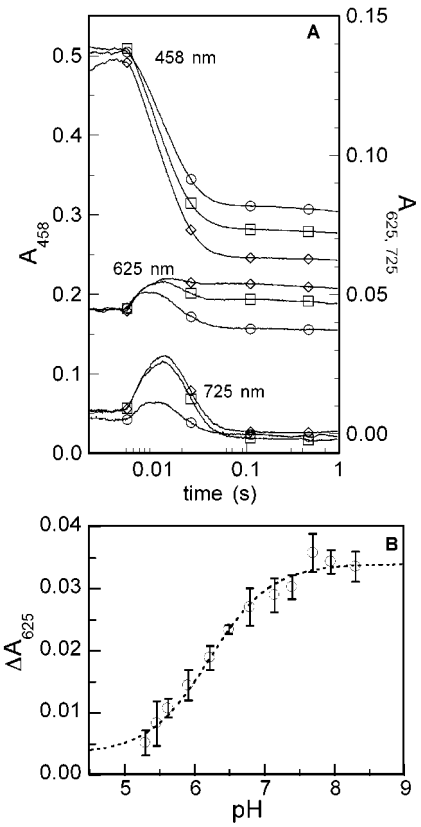

FIGURE 4: Effect of pH on the reduction of $MMOR_{ox}$ by NADH. (A) The 25 μM $MMOR_{ox}$ was allowed to react with 250 μM NADH at 4 °C. Traces recorded at 458, 625, and 725 nm are shown for pH values of 5.35 (circles), 7.10 (squares), and 8.50 (diamonds). (B) Net change in absorbance at 625 nm as a function of pH. The dashed line is a fit to eq 6.

is also evident that the maximum value of A_{725} is reduced at low pH values. The rates of the processes described in Scheme 2 are unchanged. The net change in absorbance at 625 nm between 0 and 1 s as a function of pH reflects a process having a pK_a of 6.2 ± 0.1 (Figure 4B).

Figures 5A and B display the effect of pH on the reaction of MMOR with NADH as monitored spectrophotometrically from 400 to 700 nm. Differences in the initial spectra recorded after mixing reveal pH effects on the absorbance of $MMOR_{ox}$, which arise mainly from changes in the spectrum of FAD (*24*). Comparison of spectra recorded at 1.5 s after mixing at pH 5.27 and 8.01 illustrates the different distribution of the two electrons among the FAD and [2Fe−2S] cofactors (Figure 5C). To quantify this electron distribution, the spectra were fit as a sum of the component spectra, and the results of the fit are shown in Table 3. The component spectra used in the fitting were determined at the appropriate pH. Of the five redox states accessible to the two cofactors ($FAD_{ox,\ sq,\ hq}$ and $[2Fe{-}2S]_{ox,\ red}$), only the spectra of FAD_{ox} and FAD_{hq} undergo significant pH-dependent changes (Figure 6).

Effect of pH on Relative Redox Potentials. The observed effect of pH on electron distribution in the kinetically generated $MMOR_{2e-}$ led us to investigate the effect of pH on the thermodynamic redox potentials of MMOR. Reductive titrations of $MMOR_{ox}$ were performed at varying pH values, and difference spectra were fit as sums of component difference spectra recorded at the appropriate pH. Since no redox indicator dye was included, the solution potential was unknown, and the redox potential of a particular couple was determined relative to the other redox couples of MMOR. These results are presented in Figure 7. The difference between the potentials of the [2Fe−2S] cluster and the $FAD_{sq/hq}$ couple ($E_{FeS} - E_{FAD2}$) varies from 2.8 ± 6.3 mV at pH 5.62 to 83.9 ± 11.7 mV at pH 8.01. Fitting the data to eq 6 reveals a pK_a of 6.3 ± 0.2. The value of $E_{FeS} - E_{FAD1}$ changes from −45.6 ± 3.5 to 31.1 ± 3.7 mV over the same pH range, and the corresponding pK_a value is 7.3 ± 0.1 mV. The pH-dependent difference between the two FAD couples, $E_{FAD2} - E_{FAD1}$, has an inverted bell-shaped profile with a minimum value of −93.5 ± 3.9 mV at pH 7.00 and approaches a value of ∼−50 mV at the extremes of the pH range examined. The two pK_a values derived from fits of the data are 6.6 ± 0.5 and 7.6 ± 0.9 for the low and high pH ranges, respectively (Figure 7).

Measurement of Electron Transfer by pH Jump. The pH dependence of the electron distribution among cofactors in MMOR makes possible the measurement of electron-transfer rates in the absence of other complicating factors, such as the presence of excess quantities of NAD(H). By preparing $MMOR_{2e-}$ at one pH value, it is possible to follow the redistribution of electrons following a rapid change in solution pH. Such an experiment was carried out by using the double-mixing stopped-flow method. In the first mixing

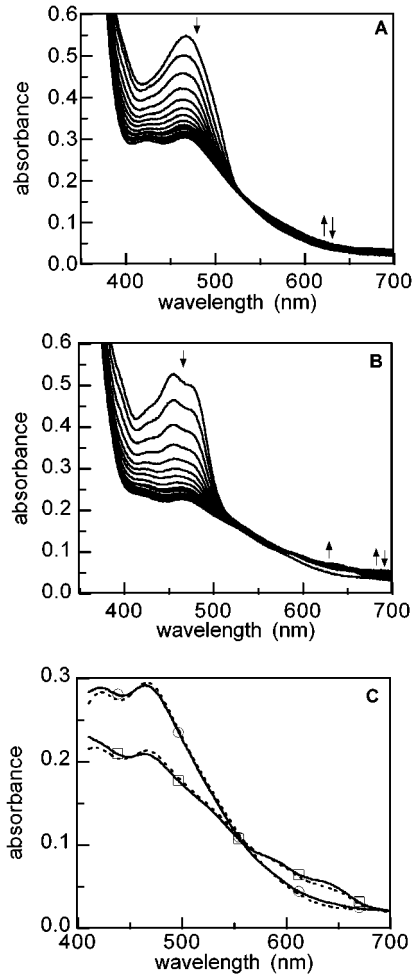

FIGURE 5: (A) Spectra recorded at ~3 ms intervals by diode array stopped-flow spectrophotometry in the first 68 ms after mixing $MMOR_{ox}$ with a 10-fold excess of NADH at pH 5.27. (B) As in (A) but at pH 8.01. (C) Spectra were recorded 1.5 s after mixing. Key: circles, pH 5.27; squares, pH 8.01. Dashed lines are fits to sums of component spectra.

Table 3: pH-Dependent Distribution of Electrons in $MMOR_{2e-}$

species	% of tot. cofactor pH 5.27	pH 8.01
$[2Fe-2S]_{ox}$	99.5	67.4
$[2Fe-2S]_{red}$	0.5	32.6
FAD_{ox}	0.3	0.3
FAD_{sq}	0.5	32.6
FAD_{hq}	99.2	67.1
$E_{FeS} - E_{FAD2}$[a]	−244 mV	−35 mV

[a] Artificial difference in redox potential between the [2Fe−2S] and FAD cofactors computed from the species distribution given in this table by application of the Nernst equation.

event, MMOR was mixed with an equimolar amount of NADH. Following a 1-s delay, a second mixing event changed the pH. The absorbance at 625 nm was followed as a function of time after the pH change, as shown in Figure 8. The traces were readily fit to a single-exponential function, and the computed rate constants were 126 ± 22 s^{-1} for jumping to a higher pH and 134 ± 5 s^{-1} for jumping to a lower pH. The rate constant determined using data for both the forward and reverse reactions is 130 ± 17 s^{-1}. In both directions, the electron transfer between FAD and [2Fe−2S] occurred with a greater rate constant than observed upon

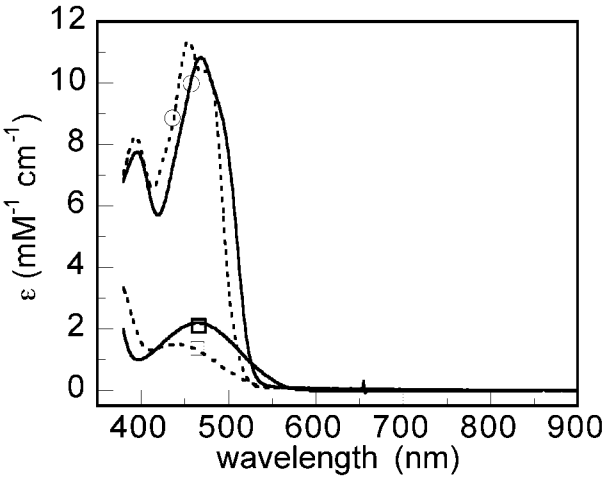

FIGURE 6: Spectra of FAD_{ox} (circles) and FAD_{hq} (squares) at pH 5.47 (solid lines) and pH 8.01 (dashed lines) (*24*).

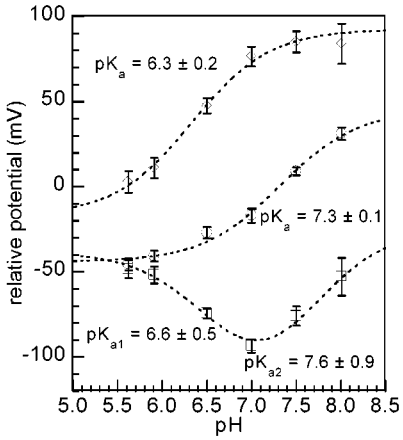

FIGURE 7: Differences between the redox potentials of MMOR at varying pH: circles, $E_{FeS} - E_{FAD1}$; squares, $E_{FAD2} - E_{FAD1}$; diamonds, $E_{FeS} - E_{FAD2}$. Dashed lines are fits of the same form as eq 6.

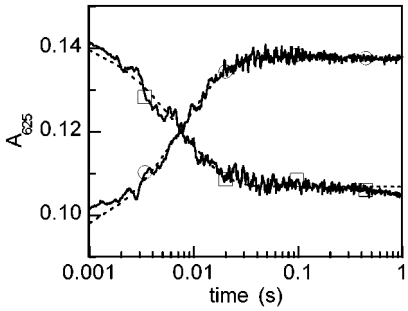

FIGURE 8: Equilibration of electrons in $MMOR_{2e-}$ following a pH jump. Absorbance at 625 nm is shown as a function of time: circles, after jump from pH 5.79 to 8.10; squares, after jump from pH 8.02 to 5.78. Dashed lines are single-exponential fits.

mixing MMOR with NADH ($k_3 = 90$ s^{-1}, Scheme 2), where electron transfer is accompanied by release of NAD^+.

DISCUSSION

Recombinant MMOR. The first high-yield recombinant system for expression of MMOR has been achieved. Good yields of pure protein with a full complement of cofactors can be obtained in a few days. A previous account detailing the expression of *M. capsulatus* (Bath) MMOR in *E. coli*

demonstrated the reconstitution of MMOR activity in cell extracts, but the yield was no greater than that from the native organism and no purification of the MMOR protein was reported (*32*). Development of a high-yielding recombinant system has made feasible the kinetic and thermodynamic studies in the present work. The amount of MMOR in *Methylosinus trichosporium* OB3b cells is ~10% of the amount of MMOH (*33*), and only small quantities of MMOR (~5−10 mg) can be purified from 100 g of *M. capsulatus* (Bath) cell paste in a routine preparation. With the recombinant system, we can easily obtain the 100 mg quantities required for extensive kinetic and thermodynamic characterization.

In addition, the purification of MMOR from the present recombinant system is more convenient than from the native organism. The protocol has fewer steps, and *E. coli* are simpler to grow than *M. capsulatus* (Bath), because the latter requires methane for growth and, even under optimal conditions, grows slowly by comparison with *E. coli*. The recombinant system also makes possible mutagenesis studies.

Redox Potentials of MMOR Cofactors. The reduction potentials of the MMOR cofactors determined here are more accurate than those reported previously (*26*). The $FAD_{ox/sq}$ potential we measured is 26 mV more negative than the published value (*26*), although the two are within experimental error of one another, given the larger error in the latter. The method used here has the advantage of treating data from many wavelengths simultaneously and generates multiple measurements of the redox potential per experiment. In addition, fitting of difference spectra allows the use of fewer parameters than would otherwise be necessary. Having fewer parameters improves the chance of finding a unique solution for the fit. Our study has also measured the potentials in the presence of several redox dyes, covering a range of 78 mV, thereby decreasing the possibility that systematic errors are introduced by a nonideal dye−protein combination.

Addition of MMOB does not affect these potentials within experimental error, consistent with other observations indicating that no complex is formed between MMOB and MMOR (*10*). The midpoint potentials for the MMOR cofactors are also unaltered in complexes with MMOH and MMOH/2MMOB. Previous studies have revealed that, for the sMMO of *M. trichosporium* (OB3b), binding of MMOR to MMOH alters the potentials of the nonheme diiron active site of MMOH (*34*, *35*). We show here for the first time that the reverse is not true; the potentials of MMOR are unchanged in the MMOH/MMOR complex.

Electron-Transfer Properties. Electron-transfer reactions involving NAD(P)H, flavin, and [2Fe−2S] cofactors have been studied in detail for other enzymes. Phthalate dioxygenase reductase (*36*) and E_3 (*37*) in particular have been well characterized. MMOR, PDR, and E_3 share similar mechanisms in their reactions with NADH. Each binds NADH, proceeds through two charge-transfer intermediates, and finally passes one electron to a [2Fe−2S] center. The existence of an MC1-type precomplex has been established for PDR but not for E_3 (*36*, *37*).

On the basis of the stopped-flow optical experiments, we propose the following model for the reduction of MMOR by NADH (Scheme 2). The initial step is rapid binding of NADH to MMOR to produce a Michaelis complex, MC1. The K_d value for this interaction is calculated to be 3.8 μM (Figure 2). Formation of MC1 does not alter the spectrum of MMOR; its existence is inferred from the kinetic behavior of the enzyme. In an earlier kinetic study of the interaction of NADH with MMOR (*28*), a precomplex of this sort was proposed on the basis of a linear double-reciprocal plot. A subsequent investigation (*29*) reported that such a complex did not exist; rather, MMOR and NADH reacted with a second-order rate constant of 2.9×10^6 M^{-1} s^{-1}. These studies were carried out at 18 °C; at this temperature, the early phases of the reaction (including CT1 formation) occur largely or completely during the dead time of the instrument, making their true rate constants difficult to determine. At 4 °C, the temperature used in this study, we find the value of CT1 formation to be 350 s^{-1} with saturating NADH. With the 2 ms dead time of our instrument approximately 50% of the optical change will be observed, enough to make an accurate determination of the rate constant. For these reasons, we stand by our proposed mechanism for MMOR reduction (Scheme 2) involving a precomplex of NADH with MMOR prior to the first observed intermediate.

Next, a conformational change is presumed to occur, with an observed rate constant of 350 s^{-1}, that gives rise to the charge-transfer interaction of CT1. Transfer of hydride from NADH to FAD ensues with a rate constant of 190 s^{-1}, yielding the CT2 species. CT2 has a more intense, lower energy charge-transfer band than CT1. The breakdown of CT2 occurs with a rate constant of 90 s^{-1}. Since this process is slower than the rate at which it is formed, CT2 builds up to appreciable concentrations under the conditions examined.

Electron transfer and release of NAD^+ are observed to occur simultaneously, affording the SQ species with reduced [2Fe−2S] and FAD_{sq}. A more complete description of the SQ state is that of an equilibrium between $FAD_{sq}/[2Fe-2S]_{red}$ and $FAD_{hq}/[2Fe-2S]_{ox}$. The spectrum of SQ shows maxima at approximately 600 and 650 nm, consistent with a neutral flavin semiquinone. This information alone does not distinguish between the possibilities that (i) the electron transfer and NAD^+ release steps are independent and coincidentally occur at similar rates, (ii) the two steps are truly coupled, or (iii) one event triggers the rapid execution of the other. Similar behavior was also observed for PDR and E_3 (*36*, *37*).

Influence of pH on Redox Properties of MMOR. Figure 4A shows the effect of pH on the reaction of MMOR with NADH. From single-wavelength stopped-flow data, it can be concluded that the kinetics of MMOR reduction by NADH are not altered as a function of pH (Figure 4A). Thus, the reduced A_{725} values at low pH measured ~10 ms after mixing (Figure 4A) are due to a lower value of ϵ_{725} for CT2 and not decreased concentrations of CT2. Although the kinetics of the reaction do not change with pH, the distribution of electrons between FAD and [2Fe−2S] in $MMOR_{2e-}$ is affected by changes in pH. The pK_a for the process affecting the final value of A_{625} is 6.2 ± 0.1 (Figure 4B).

From the data collected with the diode array, it is apparent that the spectrum of $MMOR_{ox}$ is altered by pH (initial spectra, Figures 5A and B). In Figure 5C, the changes in electron distribution are demonstrated in the final spectra. The pH effect on electron distribution is quantified in Table 3. At pH 5.27, nearly all of the MMOR is in the $FAD_{hq}/[2Fe-2S]_{ox}$ state. At pH 8.01, there is a mixture of $FAD_{hq}/[2Fe-2S]_{ox}$ and $FAD_{sq}/[2Fe-2S]_{red}$. This observation sug-

gests that the difference between the $[2Fe-2S]_{ox/red}$ and $FAD_{sq/hq}$ couples ($E_{FeS} - E_{FAD2}$) within a given molecule is diminished at low pH. This pH-dependent change in potential need not be reflected in the true thermodynamic potentials for the protein cofactors, since interprotein electron-transfer reactions cannot occur to establish equilibrium on this time scale (vide infra). Only this ΔE needs to be considered for the stopped-flow reaction, because the FAD_{ox} redox state is also inaccessible on the time scale studied.

Equilibrium titrations of MMOR at varying pH reveal that the true $E_{FeS} - E_{FAD2}$ difference is also diminished at low pH (Figure 7). At pH 8.0 the value of $E_{FeS} - E_{FAD2}$ is 83.9 mV, meaning that electron transfer from FAD_{hq} to $[2Fe-2S]_{ox}$ is favorable. At pH 5.6 this value is only 2.8 mV and there is little driving force for the same electron transfer. The pK_a values for $E_{FAD2} - E_{FAD1}$ (6.6 ± 0.5 and 7.6 ± 0.9) coincide with those found for $E_{FeS} - E_{FAD2}$ (6.3 ± 0.2) and $E_{FeS} - E_{FAD1}$ (7.3 ± 0.1), respectively. The agreement of these values is consistent with the titratable group(s) being associated with the flavin moiety. In addition, the pK_a calculated for changes in $E_{FeS} - E_{FAD2}$ compares well with the pK_a of 6.2 ± 0.1 determined in stopped-flow studies.

An artificial value for $E_{FeS} - E_{FAD2}$ under the conditions employed in the stopped-flow experiment can be calculated from the species distribution by using the Nernst equation (Table 3). Doing so reveals that $E_{FeS} - E_{FAD2}$ increases with increasing pH, consistent with the thermodynamic experiment (Figure 7). In fact, the pK_a measured in both the titration and stopped-flow experiments is identical within error ($\sim$6.3). It is not surprising, however, that the $E_{FeS} - E_{FAD2}$ values determined in titration experiments, 2.8 and 83.9 mV at low and high pH, respectively, are significantly different from those calculated from the stopped-flow data. At least three differences between the kinetic and thermodynamic experiments may contribute to this discrepancy. The major reason is that the titration experiments measure true equilibrium differences in redox potential; several minutes were allowed to elapse between the addition of reducing agent and the recording of a spectrum to ensure that equilibrium was attained. Spectra from the diode array during the stopped-flow experiment were recorded 1.5 s after mixing $MMOR_{ox}$ and NADH. On this time scale, disproportionation between molecules of $MMOR_{2e-}$ is slow, and the reaction does not reach thermodynamic equilibrium. Moreover, the stopped-flow experiments were conducted at 4 °C, whereas the titrations were performed at 25 °C. In addition, $MMOR_{ox}$ was allowed to react in the stopped-flow experiment with 10 equiv of NADH to ensure pseudo-first-order behavior. As a consequence, the derived ΔE values are measured for a mixture of species in which NAD(H) is bound to the protein. The titrations were performed in the absence of any such pyridine nucleotide.

The increase of $E_{FeS} - E_{FAD2}$ with increasing pH must arise from a decrease in E_{FAD2}, an increase in E_{FeS}, or a combination of both effects. The evidence suggests that the majority of the effect arises from a decrease in E_{FAD2}. There is no pH effect on the optical spectrum of the [2Fe−2S] cluster in either redox state, whereas the spectra of FAD_{ox} and FAD_{hq} are pH-dependent (Figure 6) (*38*). In addition, the pH dependence of $E_{FAD2} - E_{FAD1}$ shows two pK_a values (6.6 ± 0.5 and 7.6 ± 0.9), each of which is very close to a pK_a determined for one of the other ΔE values (Figure 7). It

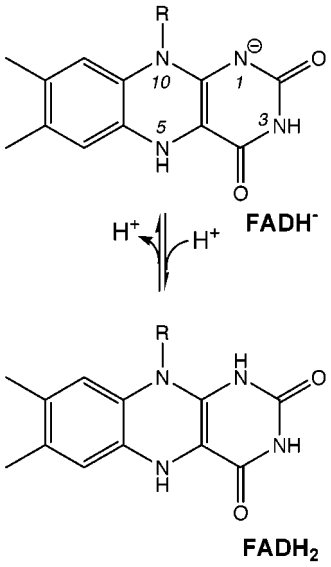

FIGURE 9: Protonation states of fully reduced FAD.

appears that there is one pK_a associated with E_{FAD2}, measured as 6.6 ± 0.5 and again as 6.3 ± 0.2, and a second pK_a associated with E_{FAD1}, measured as 7.6 ± 0.9 and a second time as 7.3 ± 0.1. By this reasoning, there is a pK_a of $\sim$7.3 affecting the value of E_{FAD1} and pK_a of $\sim$6.3 for E_{FAD2}, which is consistent with the value of 6.2 determined in the stopped-flow experiment. Furthermore, it appears that there is no macroscopic pK_a associated with E_{FeS}.

Presumably, protonation of some group(s) on, or hydrogen bonded to, the FAD isoalloxazine ring increases the $FAD_{sq/hq}$ reduction potential relative to that of the [2Fe−2S] cluster. Specifically, we propose that the N1 position of the flavin is a likely site of protonation (Figure 9). In the hydroquinone state, N1 is typically deprotonated at pH 7 and bears substantial negative charge, as judged by ^{15}N and ^{13}C NMR spectral studies for all flavoproteins that have been investigated (*39*). One-electron transfer from FAD_{hq} ($FADH^-$) to $[2Fe-2S]_{ox}$ removes this negative charge from the flavin, affording the neutral semiquinone. Protonation of N1 affords a neutral FAD_{hq} ($FADH_2$), thereby rendering electron transfer to [2Fe−2S] less favorable. Mutagenesis studies of flavodoxins also reveal that removing acidic residues in the vicinity of N1 increases the semiquinone/hydroquinone reduction potential (*40*−*42*). Protonation of the N1 site is also consistent with the observation of lower ϵ_{725} for CT2 at low pH. The charge-transfer interaction between the pyridine moiety of NAD^+ and $FADH_2$ will be much weaker than between NAD^+ and $FADH^-$. The measured pK_a of 6.2 for FAD_{hq} is within the range of values measured for the N1 position of other flavoproteins (*43*). More extensive studies could further our understanding of the molecular basis of the pH effects described above. Without additional information, however, we cannot completely rule out the possibility that pH effects occur at both FAD and [2Fe−2S] cofactors.

Intramolecular Electron Transfer. Electron transfer between FAD and [2Fe−2S], as measured by the pH jump method, occurs with a rate constant of 130 ± 17 s^{-1}. This value probably does not reflect the true rate of electron transfer. Calculations indicate that electron transfer between redox centers located 14 Å or less apart typically occurs at rates in the 10^7-10^{13} s^{-1} range (*44*). The X-ray structure of

PDR reveals the 8-CH_3 group of the flavin and Fe1 of the [2Fe−2S] cluster to be separated by 7.2 Å (*15*). This distance is well within the 14 Å range predicted to allow very rapid electron transfer, independent of other factors such as pathway or the packing density of the intervening protein. MMOR is expected to have a similar structure, and although the flavin-to-[2Fe−2S] distance may be greater in MMOR than in PDR, it is likely to be less than 14 Å. We therefore conclude that the relatively slow rate constant for electron transfer in MMOR reflects a rate-limiting, preceding step such as a conformational change of the protein, perhaps one that is coupled with proton transfer. The link between the FAD and [2Fe−2S] domains of MMOR may be sufficiently flexible to allow these two cofactors to be positioned such that rapid tunneling cannot occur in all conformations.

The greater electron-transfer rate constant measured in the pH jump, compared to the constant pH (90 s^{-1}, k_3 in Scheme 2), experiments suggests that NAD^+ release is rate-limiting in the latter case. In the pH jump experiment, a minority fraction of $MMOR_{2e-}$ has bound NAD^+, owing to the weak binding constant ($K_d \sim 70$ μM) and the use of equimolar concentrations of $MMOR_{2e-}$ and NAD^+.

Conclusion. The studies of intramolecular electron transfer in the sMMO system described here, coupled with forthcoming structural information about the [2Fe−2S] domain of MMOR (*24*, *45*), will provide a detailed understanding of intermolecular electron transfer in the sMMO system (*10*). Electron-transfer steps in the overall catalytic cycle of sMMO have been the subject of little work until now. With the availability of large quantities of recombinant MMOR, this previously neglected aspect of the sMMO system can now be investigated. For not only is the hydroxylation of the C−H bond in methane a remarkable feat of chemistry, but the carefully orchestrated intra- and interprotein electron transfer steps are as well. Knowledge of these processes will not only enrich our understanding of the sMMO system but will also contribute to the general field of electron transfer in biology.

REFERENCES

1. Mancinelli, R. L. (1995) *Annu. Rev. Microbiol. 49*, 581−605.
2. Tsien, H.-C., Brusseau, G. A., Hanson, R. S., and Wackett, L. P. (1989) *Appl. Environ. Microbiol. 55*, 3155−3161.
3. Brockman, F. J., Payne, W., Workman, D. J., Soong, A., Manley, S., and Hazen, T. C. (1995) *J. Hazard. Mater. 41*, 287−298.
4. Colby, J., and Dalton, H. (1978) *Biochem. J. 171*, 461−468.
5. Feig, A. L., and Lippard, S. J. (1994) *Chem. Rev. 94*, 759−805.
6. Wallar, B. J., and Lipscomb, J. D. (1996) *Chem. Rev. 96*, 2625−2657.
7. Valentine, A. M., and Lippard, S. J. (1997) *J. Chem. Soc., Dalton Trans.*, 3925−3931.
8. Merkx, M., Kopp, D. A., Sazinsky, M. H., Blazyk, J. L., Müller, J., and Lippard, S. J. (2001) *Angew. Chem., Int. Ed. 40*, 2782−2807.
9. Nguyen, H.-H. T., Elliott, S. J., Yip, J. H.-K., and Chan, S. I. (1998) *J. Biol. Chem. 273*, 7957−7966.
10. Gassner, G. T., and Lippard, S. J. (1999) *Biochemistry 38*, 12768−12785.
11. Liu, K. E., Valentine, A. M., Wang, D., Huynh, B. H., Edmondson, D. E., Salifoglou, A., and Lippard, S. J. (1995) *J. Am. Chem. Soc. 117*, 10174−10185.
12. Valentine, A. M., Stahl, S. S., and Lippard, S. J. (1999) *J. Am. Chem. Soc. 121*, 3876−3887.
13. Shu, L., Nesheim, J. C., Kauffmann, K., Münck, E., Lipscomb, J. D., and Que, L., Jr. (1997) *Science 275*, 515−518.
14. Miller, V. P., Thorson, J. S., Ploux, O., Lo, S. F., and Liu, H.-W. (1993) *Biochemistry 32*, 11934−11942.
15. Correll, C. C., Batie, C. J., Ballou, D. P., and Ludwig, M. L. (1992) *Science 258*, 1604−1610.
16. Zhou, N.-Y., Jenkins, A., Chan Kwo Chion, C. K. N., and Leak, D. J. (1998) *FEBS Lett. 430*, 181−185.
17. Nordlund, I., Powlowski, J., and Shingler, V. (1990) *J. Bacteriol. 172*, 6826−6833.
18. Mason, J. R., and Cammack, R. (1992) *Annu. Rev. Microbiol. 46*, 277−305.
19. Butler, C. S., and Mason, J. R. (1997) *Adv. Microbiol. Physiol. 38*, 47−84.
20. Massey, V. (1957) *J. Biol. Chem. 229*, 763−770.
21. Stookey, L. L. (1970) *Anal. Chem. 42*, 779−781.
22. Stainthorpe, A. C., Murrell, J. C., Salmond, G. P. C., Dalton, H., and Lees, V. (1989) *Arch. Microbiol. 152*, 154−159.
23. Coufal, D. E., Blazyk, J. L., Whittington, D. A., Wu, W. W., Rosenzweig, A. C., and Lippard, S. J. (1999) *Eur. J. Biochem. 267*, 2174−2185.
24. Blazyk, J. L., Gassner, G. T., and Lippard, S. J. (2001), manuscripts in preparation.
25. Colby, J., and Dalton, H. (1979) *Biochem. J. 177*, 903−908.
26. Lund, D., and Dalton, H. (1985) *Eur. J. Biochem. 147*, 291−296.
27. Walters, K. J., Gassner, G. T., Lippard, S. J., and Wagner, G. (1999) *Proc. Natl. Acad. Sci. U.S.A. 96*, 7877−7882.
28. Lund, J., Woodland, M. P., and Dalton, H. (1985) *Eur. J. Biochem. 147*, 297−305.
29. Green, J., and Dalton, H. (1989) *Biochem. J. 259*, 167−172.
30. Barshop, B. A., Wrenn, R. F., and Frieden, C. (1983) *Anal. Biochem. 130*, 134−145.
31. Wachsstock, D. H., and Pollard, T. D. (1994) *Biophys. J. 67*, 1260−1273.
32. West, C. A., Salmond, G. P. C., Dalton, H., and Murrell, J. C. (1992) *J. Gen. Microbiol. 138*, 1301−1307.
33. Fox, B. G., Froland, W. A., Dege, J. E., and Lipscomb, J. D. (1989) *J. Biol. Chem. 264*, 10023−10033.
34. Paulsen, K. E., Liu, Y., Fox, B. G., Lipscomb, J. D., Münck, E., and Stankovich, M. T. (1994) *Biochemistry 33*, 713−722.
35. Liu, Y., Nesheim, J. C., Paulsen, K. E., Stankovich, M. T., and Lipscomb, J. D. (1997) *Biochemistry 36*, 5223−5233.
36. Gassner, G., Wang, L., Batie, C., and Ballou, D. P. (1994) *Biochemistry 33*, 12184−12193.
37. Gassner, G. T., Johnson, D. A., Liu, H.-W., and Ballou, D. P. (1996) *Biochemistry 35*, 7752−7761.
38. Blazyk, J. L., Kopp, D. A., and Lippard, S. J. (2001), unpublished data.
39. Müller, F. (1992) in *Chemistry and Biochemistry of Flavoenzymes* (Müller, F., Ed.) pp 557−595, CRC Press, Boca Raton, FL.
40. Geoghegan, S. M., Mayhew, S. G., Yalloway, G. N., and Butler, G. (2000) *Eur. J. Biochem. 267*, 4434−4444.
41. Hoover, D. M., Drennan, C. L., Metzger, A. L., Osborne, C., Weber, C. H., Pattridge, K. A., and Ludwig, M. L. (1999) *J. Mol. Biol. 294*, 725−743.
42. Zhou, Z., and Swenson, R. P. (1996) *Biochemistry 35*, 15980−15988.
43. Franken, H.-D., Rüterjans, H., and Müller, F. (1984) *Eur. J. Biochem. 138*, 481−489.
44. Page, C. C., Moser, C. C., Chen, X., and Dutton, P. L. (1999) *Nature 402*, 47−52.
45. Müller, J., Lugovskoy, A. A., Wagner, G., and Lippard, S. J. (2001) *Biochemistry*, in press.

BI015556T